Hindawi
International Journal of Aerospace Engineering
Volume 2022, Article ID 3069092, 16 pages
https://doi.org/10.1155/2022/3069092

Research Article

Neural Network Based Adaptive Backstepping Control for Electro-Hydraulic Servo System Position Tracking

Zhenshuai Wan, Longwang Yue, and Yu Fu

School of Mechanical and Electrical Engineering, Henan University of Technology, Zhengzhou 450001, China

Correspondence should be addressed to Zhenshuai Wan; wanzhenshuai@haut.edu.cn

Received 21 June 2022; Revised 17 August 2022; Accepted 25 August 2022; Published 5 September 2022

Academic Editor: Giovanni Palmerini

The modeling uncertainties and external disturbances of electro-hydraulic servo system (EHSS) deteriorate the system's trajectory tracking performance. To cope with this issue, an adaptive backstepping controller based on neural network (NN) is proposed in this paper. A radial-basis-function neural network (RBF NN) is constructed to approximate the lumped uncertainties caused by modeling uncertainties and external disturbances, where the adaptive law is adopted to adjust controller parameters online. The backstepping control is used to eliminate mismatched nonlinear terms and stabilize the system. The dynamic surface control (DSC) is adopted to handle the "explosion of complexity" problem of backstepping method and reduce the computational burden. Compared to the traditional backstepping control, the proposed control scheme improves the steady-state tracking precision and makes the control signal smaller. In addition, the stability analysis shows that the tracking error can asymptotically converge to zero in the face of time-varying unknown dynamics. Simulation and experiment results demonstrate the effectiveness of the controller in term of tracking accuracy and disturbance rejection in comparison with other controllers for the EHSS.

1. Introduction

Electro-hydraulic servo system (EHSS) is widely used in industrial fields due to the excellent advantages of high power to weight ratio, large driving force, fast dynamic response performance, and high reliability [1–5]. Such especial features increase the application of EHSS in high speed and heavy load situation, such as vehicle active suspension [6], robotic manipulator [7], metal forming equipment [8], aerospace [9–11], and motion simulator [12]. However, due to the drawbacks of fluid compressibility, oil viscosity, nonlinear friction force, dead-zone characteristic, hysteresis, external disturbance, flow pressure characteristics, and parameter uncertainties [13–15], the EHSS usually cannot achieve high precision positioning tracking. Furthermore, the nonlinear dynamic behavior and external disturbance are unknown or not measured in practical application. Owing to the immeasurability of the disturbance, it is necessary to estimate the disturbance using adaptive or estimation algorithms [16]. Hence, various mathematical model and controller design have been investigated to cope with the uncertainties and disturbances in EHSS [17].

The classical proportional-integral-derivative (PID) controller is widely used in process control since its simple algorithm, good stability, and good reliability [18]. Nevertheless, the parameters of PID controller cannot satisfy variable working condition. To deal with this problem, intelligent optimization algorithms are introduced into the PID controller to obtain strong robust performance when the working condition changes or the parameters change [19]. However, the hybrid control scheme increases computational complexity and parameter adjustment process [20]. The feedback linearization needs an exact mathematical model to design a nonlinear control law for eliminating the

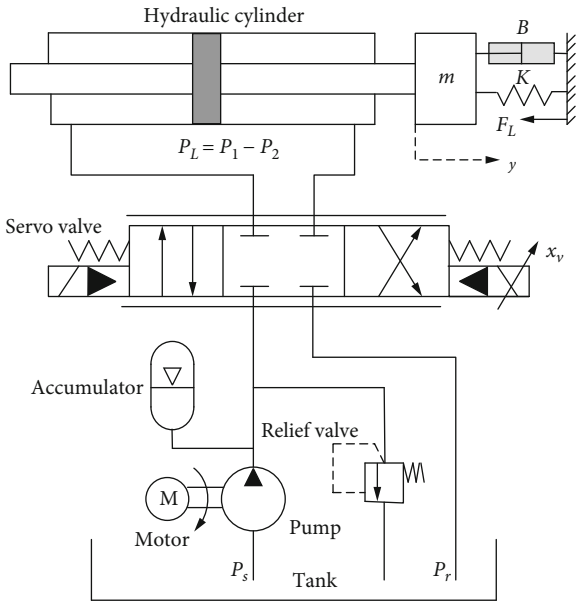

Figure 1: The schematic diagram of EHSS.

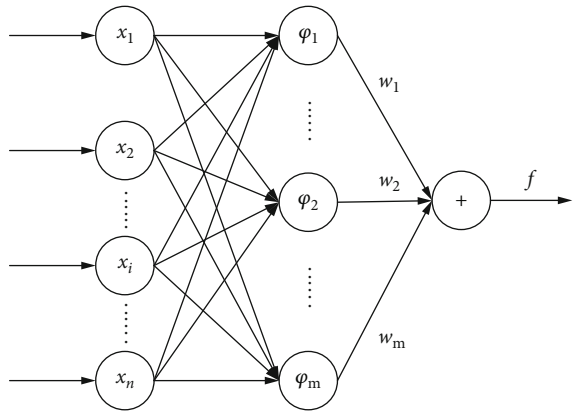

Figure 2: The structure of RBF NN.

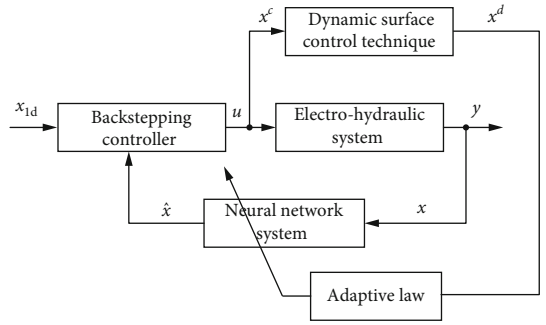

Figure 3: Block diagram of the control system.

nonlinear disturbance. Nevertheless, it needs state feedback information in real time, such as the velocity and pressure signals of EHSS [21]. From a practical perspective, this restricts the application of feedback linearization when only the position signal is measured. In addition, accurate model is hardly constructed for EHSS in presence of various dynamic behaviors and external disturbances. Considering the inherent nonlinearities and external disturbances in EHSS, traditional constant-gain controllers have become inadequate.

To handle modeling uncertainties and external disturbances, many nonlinear control methods have been proposed, such as adaptive control [22–24], sliding mode control [25–27], backstepping control [28, 29], and NN control [30–32]. Adaptive control adopts the designed adaptive law to estimate unknown but constant parameters and to improve the tracking accuracy. However, it cannot guarantee system stability when facing large unmodeled disturbances. Wang presented an approximation-free controller based on prescribed performance function technology rather than function approximation method for the tracking control of nonlinear helicopter with unknown dynamics, where the computational burden is greatly reduced [33]. Chen et al. presented an adaptive robust control scheme to deal with the complicated nonlinear dynamics and modeling uncertainties of hydraulic system, which combine adaptive control and robust control to realize accurate trajectory tracking and good robust performance [34]. The sliding mode control has the advantage of robustness to external disturbances and provides a systematic approach for maintaining stability in the face of modeling inaccuracies and uncertainties. However, chattering phenomenon, equivalent control law design, and the boundary uncertainty restrict its practical application. Cheng et al. put forward a novel sliding mode control method based on the fractional-order PID sliding surface and state observe for EHSS subjected to strong nonlinearities and parametric uncertainties, and chattering problem was finally reduced [35]. The backstepping control is an effective control method for nonlinear systems. However, the "explosion of complexity" caused by the repeated differentiation of virtual control signal at each step limits its applications. To overcome this issue, DSC method is proposed to eliminate "explosion of complexity" and guarantee satisfactory dynamic behavior [36]. Due to the outstanding advantages including learning and generalization abilities, nonlinear mapping, and parallelism computation, the NN control can reconstruct complicated nonlinear function effectively [23, 37]. Yang et al. presented a NN-based adaptive dynamic surface asymptotic tracking controller to dispose the parametric uncertainties of hydraulic robotic system, where NN approximate error and actuator's uncertainties are addressed by the nonlinear robust control law with adaptive gains [38]. Li et al. proposed an adaptive NN control scheme to improve the testing performance of dynamically substructured systems, and this method does not require any information of the plant model and disturbance model due to the online learning ability of NN [39].

Motivated by the abovementioned control strategy, NN-based adaptive backstepping control is presented for EHSS position tracking. The backstepping control is utilized to handle the nonlinearities and ensure the stability and good tracking performance. The NN is used to approximate the unknown and continuous function in the design process caused by modeling uncertainties and external disturbances,

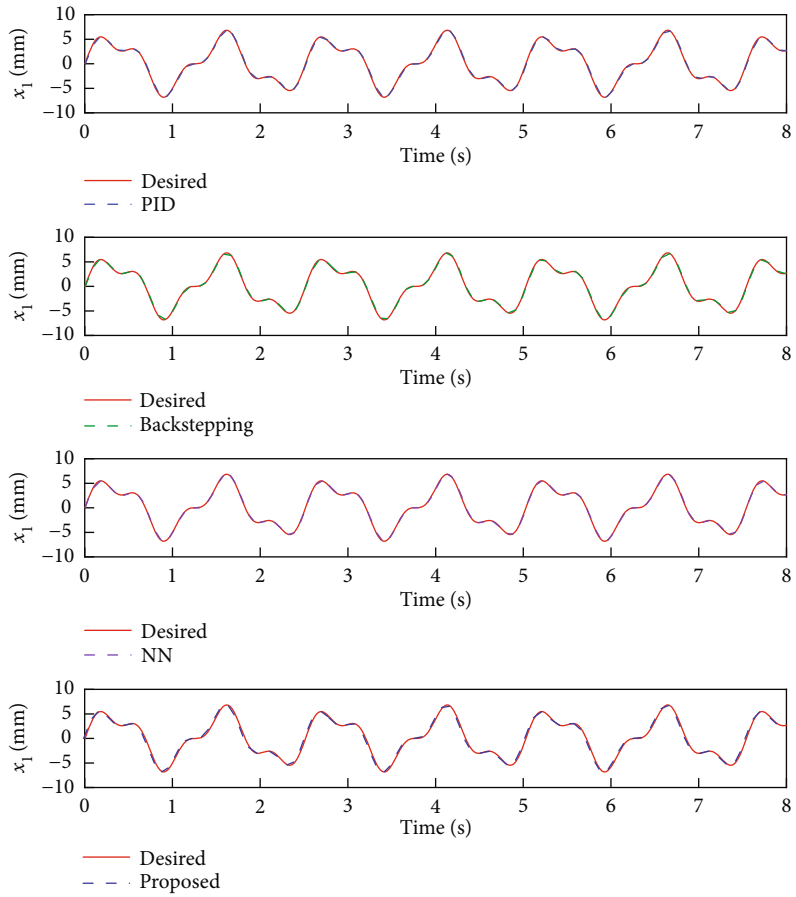

Figure 4: Tracking performance of multifrequency sine signal.

where the adaptive law is proposed to handle the parameter variations by adjusting the parameters of NN online. The DSC method is adopted to eliminate "explosion of complexity" phenomenon. The main contributions of this paper are summarized as follows: (1) A novel NN adaptive backstepping controller is proposed for electro-hydraulic servo system position tracking. (2) With the incorporation of DSC in backstepping, the proposed controller avoids the "explosion of complexity" problem. (3) The proposed controller simultaneously obtains good asymptotic stability and high tracking precision with the help of adaptive control law.

This paper is organized as follows. Dynamic model of EHSS is presented in Section 2. Section 3 shows the detailed controller design procedure and the main theoretical results. Sections 4 and 5 give simulation and experiment verification results, respectively. Finally, conclusions are provided in Section 6.

2. Dynamic Model of EHSS

The schematic diagram of EHSS is shown in Figure 1. The pump controlled by motor delivers hydraulic fluid oil from the tank to the rest of the hydraulic components. The accumulator acts as an auxiliary source of energy in case of an abrupt need for additional power. The relief valve restricts the maximum operating pressure. The servo valve generates control signal by adjusting the spool position. The hydraulic actuator drives load at desired direction and position. Force and position signals of hydraulic cylinder are obtained from the sensors and used for feedback control.

The dynamic equation of servo valve can be modeled as

$$x_v = K_{sv} u, \tag{1}$$

where x_v is the spool displacement of the servo valve, K_{sv} is the servo valve gain, and u is the control input of the servo valve.

The flow rate of the servo valve is defined as

$$Q_L = C_d w x_v \sqrt{\frac{P_s - \text{sign}\,(x_v) P_L}{\rho}}, \tag{2}$$

where Q_L is the flow rate of the servo valve, C_d is the flow discharge coefficient, w is the area gradient of the servo valve, x_v is the spool displacement of the servo valve, P_s and P_L are the supply and return oil pressure, and ρ is the fluid oil density. P_s and P_L are defined as $P_s = P_1 + P_2$ and $P_L = P_1 - P_2$. P_1 and P_2 are the pressure in the actuator chambers.

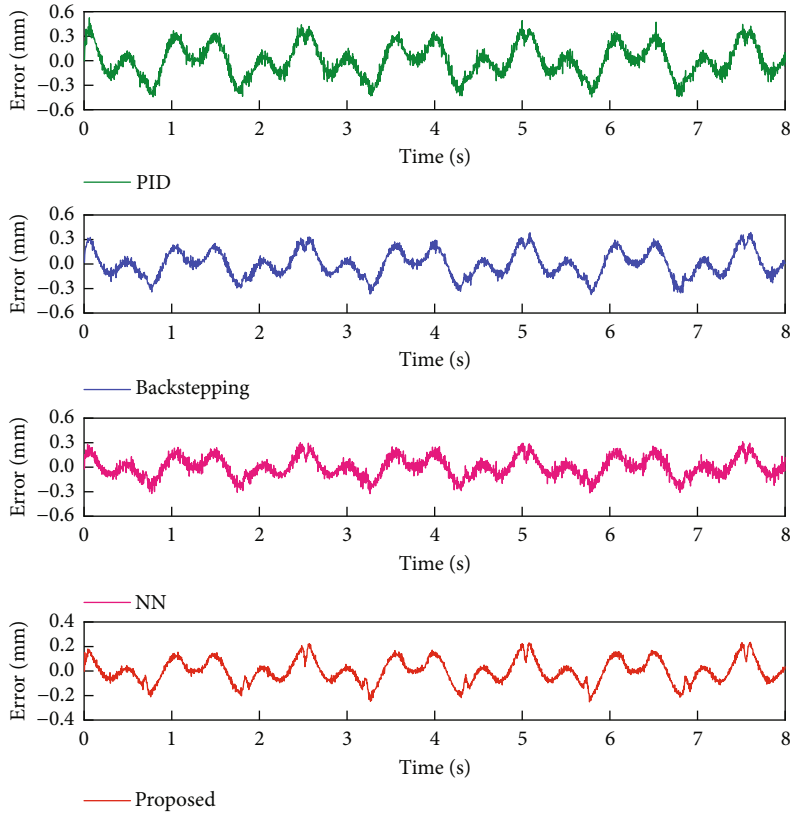

Figure 5: Tracking error of multifrequency sine signal.

Table 1: Performance indicators for multifrequency sine signal.

Indices	M_e	μ	σ
PID	0.5252	0.1594	0.1124
Backstepping	0.3855	0.1260	0.0905
NN	0.3243	0.1006	0.0719
Proposed	0.2515	0.0762	0.0570

The pressure dynamic equation of hydraulic cylinder can be established as

$$\dot{P}_L = -\frac{4\beta_e A}{V_t}\dot{y} - \frac{4\beta_e C_{tl}}{V_t}P_L + \frac{4\beta_e C_d w x_v}{V_t}\sqrt{\frac{P_s - \text{sign}\,(x_v)P_L}{\rho}}, \tag{3}$$

where A is the pressure area of the piston, y is the displacement of load, V_t is the total volume of actuator, β_e is fluid buck modulus, and C_{tl} is the total leakage coefficient.

According to the Newton's second law, the dynamics equation of hydraulic actuator can be written as

$$m\ddot{y} = P_L A - Ky - B\dot{y} - F_L, \tag{4}$$

where m is the mass of the piston, K is the load spring constant, B is the viscous damping coefficient, and F_L is the load force.

Define state variables as $[x_1, x_2, x_3]^T = [y, \dot{y}, P_L A]$, and then, the state space form of EHSS can be formulated as

$$\begin{aligned}
\dot{x}_1 &= x_2,\\
\dot{x}_2 &= \frac{1}{m}(x_3 - Kx_1 - Bx_2 - F_L),\\
\dot{x}_3 &= -\frac{4\beta_e A^2}{V_t}x_2 - \frac{4\beta_e C_{tl}}{V_t}x_3 + \frac{4\beta_e C_d w K_{sv} u A}{V_t}\sqrt{\frac{P_s - \text{sign}\,(u)x_3}{\rho A}}.
\end{aligned} \tag{5}$$

In practice, the hydraulic parameters C_d, ρ, K, B, β_e, and C_{tl} are uncertain constants. In addition, the F_L is a bounded time varying driving force. Then, Equation (5) can be rewritten as

$$\begin{aligned}
\dot{x}_1 &= g_1(x_1)x_2 + f_1(x_1),\\
\dot{x}_2 &= g_2(x_1, x_2)x_3 + f_2(x_1, x_2),\\
\dot{x}_3 &= g_3(x_1, x_2, x_3)u + f_3(x_1, x_2, x_3).
\end{aligned} \tag{6}$$

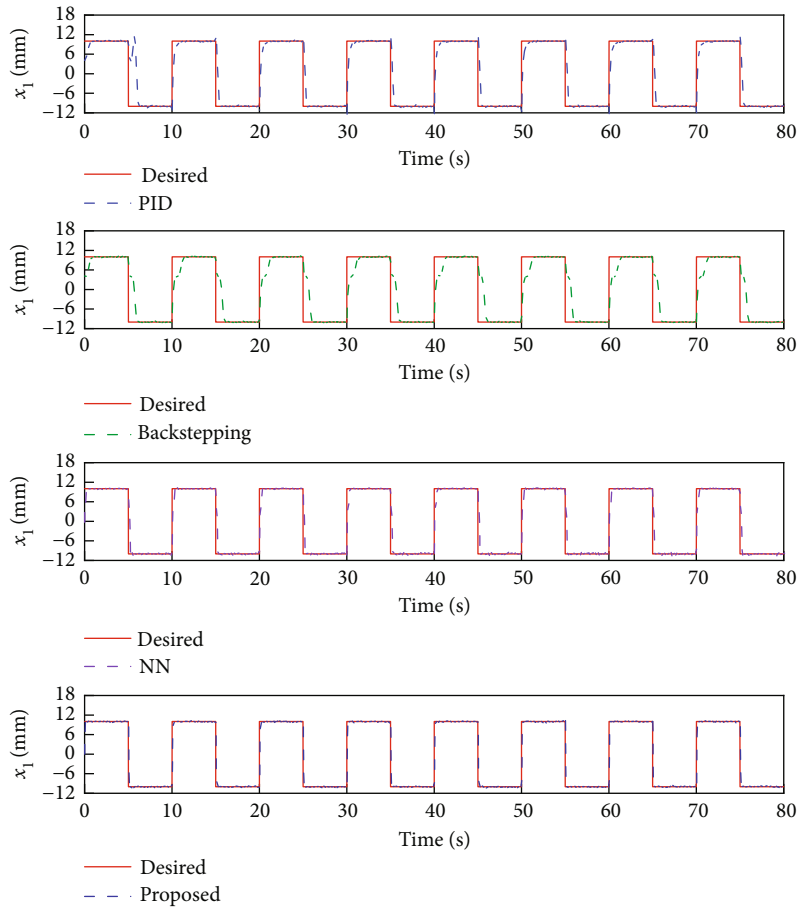

Figure 6: Tracking performance of square signal.

Table 2: Performance indicators for square signal.

Indices	M_e	μ	σ
PID	0.0131	0.0040	0.0028
Backstepping	0.0096	0.0032	0.0023
NN	0.0081	0.0025	0.0018
Proposed	0.0063	0.0019	0.0014

The model functions are described as

$$\begin{aligned} g_1(x_1) &= 1, f_1(x_1) = d_1, g_2(x_1, x_2) = \frac{1}{m}, \\ f_2(x_1, x_2) &= -\frac{K}{m}x_1 - \frac{B}{m}x_2 - \frac{F_L}{m} + d_2, \\ g_3(x_1, x_2, x_2) &= \frac{4\beta_e C_d \mathrm{wK_{sv}} A}{V_t}\sqrt{\frac{P_s - \mathrm{sign}\,(u)x_3}{\rho A}}, \\ f_3(x_1, x_2, x_2) &= -\frac{4\beta_e A^2}{V_t}x_2 - \frac{4\beta_e C_{\mathrm{tl}}}{V_t}x_3 + d_3, \end{aligned} \tag{7}$$

where d_1, d_2, and d_3 are lumped uncertain terms including modeling uncertainties and external disturbances.

3. Controller Design

For EHSS, the main goal is to design a controller to ensure that the system output can track the desired trajectory as much as possible. At the same time, all signals in closed loop system are ultimately bounded.

3.1. NN-Based Unknown Dynamic Estimation. The function approximation properties of NN guarantee that any smooth function can be approximated arbitrarily by appropriate weights and thresholds [40]. In this paper, the RBF NN is employed to deal with the modeling uncertainties and external disturbance in the dynamics of EHSS. The structure of RBF NN is shown in Figure 2.

The identification model based on RBF NN is presented as

$$f(\boldsymbol{X}) = \boldsymbol{W}^T \boldsymbol{\Phi}(\boldsymbol{X}), \tag{8}$$

where $\boldsymbol{X} = [x_1, x_2, \cdots, x_n]^T$ and $f(\boldsymbol{X})$ are the input vector and output vector, $\boldsymbol{W} = [w_1, w_2, \cdots, w_m]$ is the adjustable parameter vector, and $\boldsymbol{\Phi} = [\varphi_1, \varphi_2, \cdots, \varphi_{\mathrm{m}}]$ is the basis function.

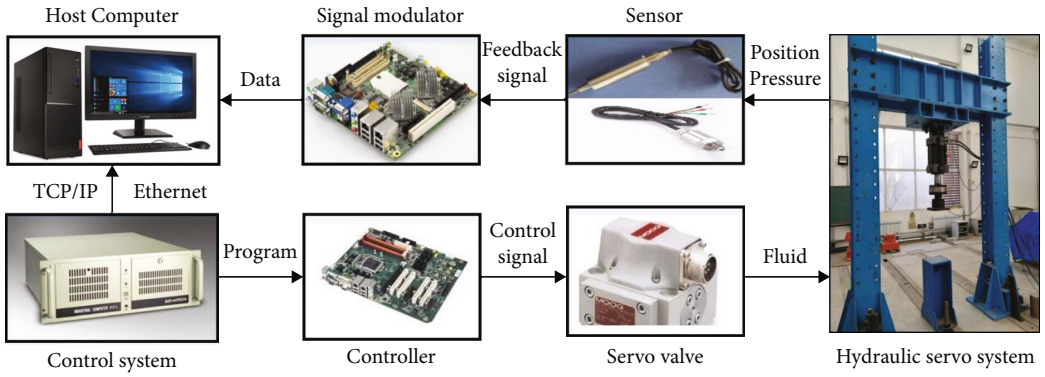

Figure 7: Electro-hydraulic servo system experimental platform.

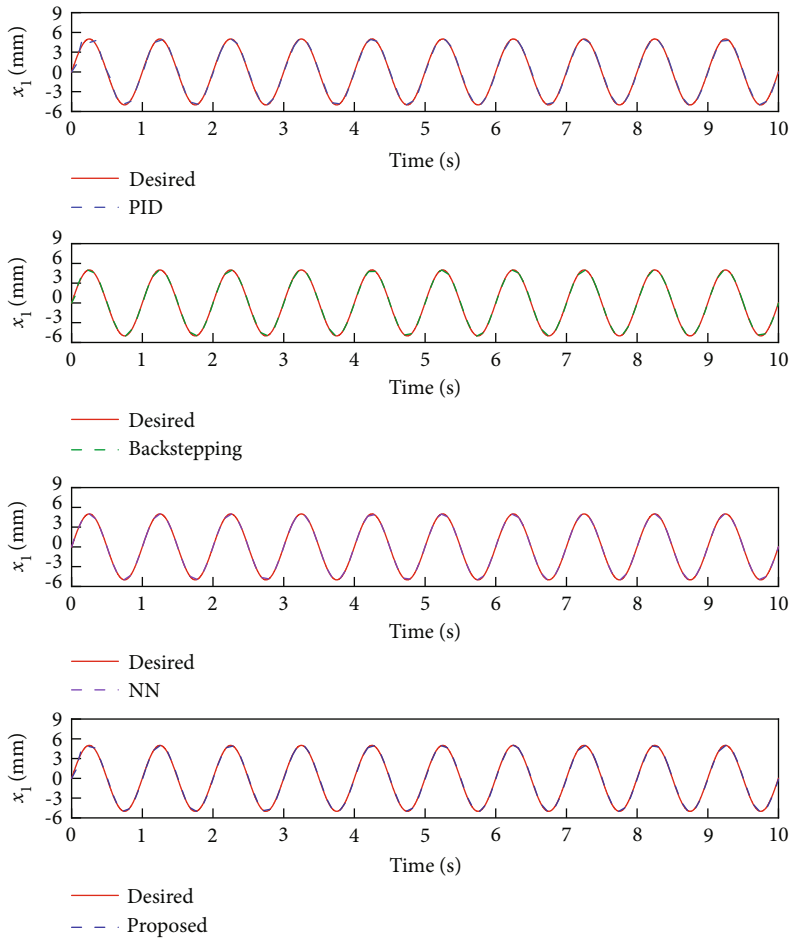

Figure 8: Tracking performance of sine signal.

The commonly used basis function is Gaussian function, which is defined as

$$\varphi_j(\boldsymbol{X}) = \exp\left(-\frac{\|\boldsymbol{X} - c_j\|}{2\sigma_j^2}\right), \tag{9}$$

where c_j and σ_j denote the center vector and width of Gaussian function, respectively.

As mentioned in [41], for any given unknown continuous function $f(\boldsymbol{X})$ on a compact set $\Omega_X \in R^n$ and an arbitrary ε_M, there exists an optimal parameter vector $\boldsymbol{W}^{*T}$ such that

$$\sup_{X \in \Omega_X} \left| \boldsymbol{W}^{*T} \boldsymbol{\Phi}(\mathbf{x}) - f(\boldsymbol{X}) \right| \leq \varepsilon_M, \tag{10}$$

where ε_M denotes the reconstruction error that is inevitably generated.

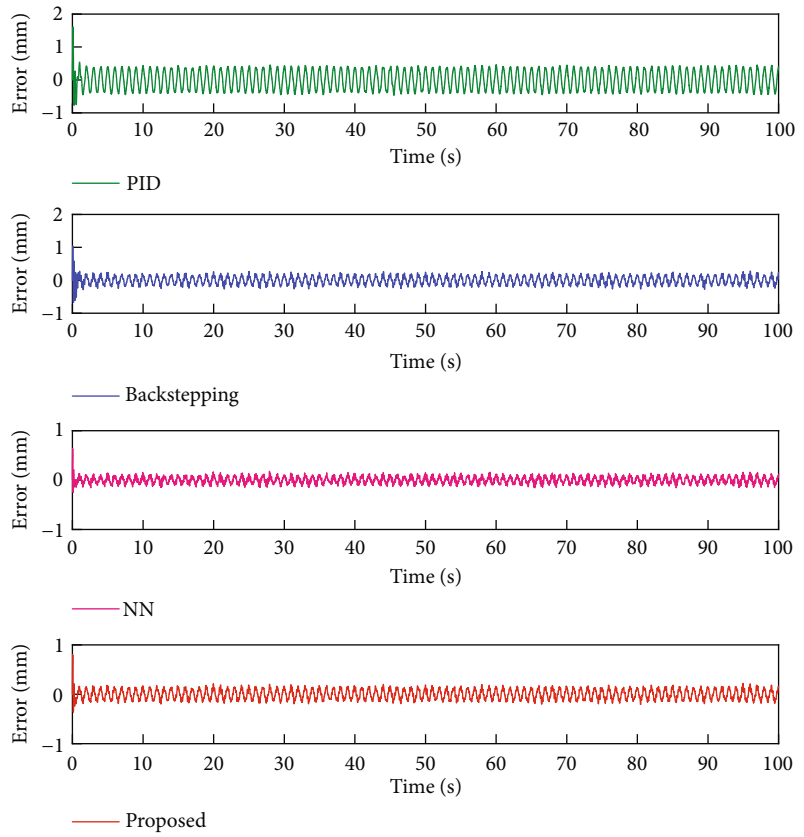

Figure 9: Tracking error of sine signal.

3.2. Controller Design. Step 1: Considering the first equation in (6) and using RBF NN to approximate $f_1(x_1)$, it yields

$$\dot{x}_1 = g_1(x_1)x_2 + f_1(x_1) = g_1(x_1)x_2 + \boldsymbol{W}_1^{*T}\boldsymbol{\Phi}_1(\boldsymbol{X}_1) + \varepsilon_1, \quad (11)$$

where $\boldsymbol{W}_1^*$ and ε_1 are optimal weight vector and approximation error, respectively.

Define the tracking error

$$e_1 = x_1 - x_{1d}, \quad (12)$$

where x_{1d} is the desired trajectory.

The virtual control is chosen as

$$x_2^d = \frac{\widehat{\boldsymbol{W}}_1^T\boldsymbol{\Phi}_1(\boldsymbol{X}_1) - k_1e_1 + \dot{x}_{1d}}{g_1}, \quad (13)$$

where $\widehat{\boldsymbol{W}}_1$ is the estimation of $\boldsymbol{W}_1^*$ and k_1 is the positive design constant.

Introduce a new state variable x_2^c, and let x_2^d pass through a first-order filter

$$\begin{aligned} \alpha_2\dot{x}_2^c + x_2^c &= x_2^d, \\ x_2^c(0) &= x_2^d(0), \end{aligned} \quad (14)$$

where α_2 is the positive time constant.

Define $e_2 = x_2 - x_2^c$, and then, the time derivative of e_1 is obtained as

$$\begin{aligned} \dot{e}_1 &= \dot{x}_1 - \dot{x}_{1d} = \widehat{\boldsymbol{W}}_1^T\boldsymbol{\Phi}_1(\boldsymbol{X}_1) + \varepsilon_1 + x_2 - \dot{x}_{1d} \\ &= \tilde{\boldsymbol{W}}_1^T\boldsymbol{\Phi}_1(\boldsymbol{X}_1) + \varepsilon_1 - k_1e_1 + e_2 + \left(x_2^c - x_2^d\right), \end{aligned} \quad (15)$$

where $\tilde{\boldsymbol{W}}_1 = \boldsymbol{W}_1^* - \widehat{\boldsymbol{W}}_1$.

To remove the effect of the known error $x_2^c - x_2^d$, the compensation signal is designed as

$$\begin{aligned} \dot{z}_1 &= -k_1z_1 + z_2 + g_1z_2 + g_1\left(x_2^c - x_2^d\right), \\ z_1(0) &= 0, \end{aligned} \quad (16)$$

where z_2 will be defined in the next step.

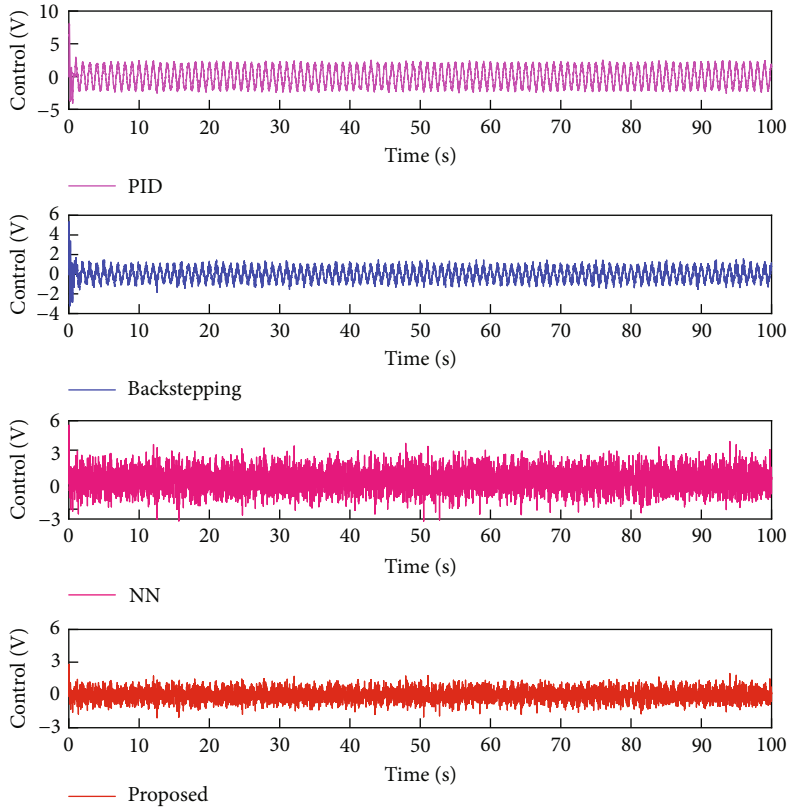

Figure 10: Control signal of sine signal.

The compensation error signal is described as

$$v_1 = e_1 - z_1. \tag{17}$$

The prediction error is defined as

$$\bar{z}_1 = x_1 - \hat{x}_1. \tag{18}$$

Then, the NN estimation model is constructed as

$$\begin{aligned} \dot{\hat{x}}_1 &= \hat{\boldsymbol{W}}_1^T \boldsymbol{\Phi}_1(\boldsymbol{X}_1) + g_1 x_2 + \beta_1 \bar{z}_1, \\ \hat{x}_1(0) &= x_1(0), \end{aligned} \tag{19}$$

where β_1 is the positive design constant.

The adaptive law of RBF NN is designed as

$$\dot{\hat{\boldsymbol{W}}}_1 = \gamma_1 \left[(v_1 + \gamma_{z1} \bar{z}_1) \boldsymbol{\Phi}_1(\boldsymbol{X}_1) - \delta_1 \hat{\boldsymbol{W}}_1 \right], \tag{20}$$

where γ_1, γ_{z1}, and δ_1 are the positive design constants.

Step 2: Considering the second equation in (6) and using RBF NN to approximate $f_2(x_2)$, it yields

$$\dot{x}_1 = g_2(x_1, x_2) x_2 + f_1(x_1, x_2) = g_1(x_1, x_2) x_2 + \boldsymbol{W}_2^{*T} \boldsymbol{\Phi}_2(\boldsymbol{X}_2) + \varepsilon_2, \tag{21}$$

where $\boldsymbol{W}_2^*$ and ε_2 are optimal weight vector and approximation error, respectively.

Define the tracking error

$$e_2 = x_2 - x_2^c. \tag{22}$$

The virtual control is chosen as

$$x_3^d = \frac{\hat{\boldsymbol{W}}_2^T \boldsymbol{\Phi}_2(\boldsymbol{X}_2) - k_2 e_2 - g_1 e_1 + \dot{x}_2^c}{g_2}, \tag{23}$$

where $\hat{\boldsymbol{W}}_2$ is the estimation of $\boldsymbol{W}_2^*$ and k_2 is the positive design constant.

Introduce a new state variable x_3^c, and let x_3^d pass through a first-order filter

$$\begin{aligned} \alpha_3 \dot{x}_3^c + x_3^c &= x_3^d, \\ x_3^c(0) &= x_3^d(0), \end{aligned} \tag{24}$$

where α_3 is the positive time constant.

Define $e_3 = x_3 - x_3^c$, then, the time derivative of e_2 is obtained as

$$\begin{aligned} \dot{e}_2 &= \dot{x}_2 - \dot{x}_2^c = \hat{\boldsymbol{W}}_2^T \boldsymbol{\Phi}_2(\boldsymbol{X}_2) + \varepsilon_2 + x_2 - \dot{x}_2^c \\ &= \tilde{\boldsymbol{W}}_2^T \boldsymbol{\Phi}_2(\boldsymbol{X}_2) + \varepsilon_2 - k_2 e_2 - e_1 + e_3 + \left(x_3^c - x_3^d \right), \end{aligned} \tag{25}$$

where $\tilde{\boldsymbol{W}}_2 = \boldsymbol{W}_2^* - \hat{\boldsymbol{W}}_2$.

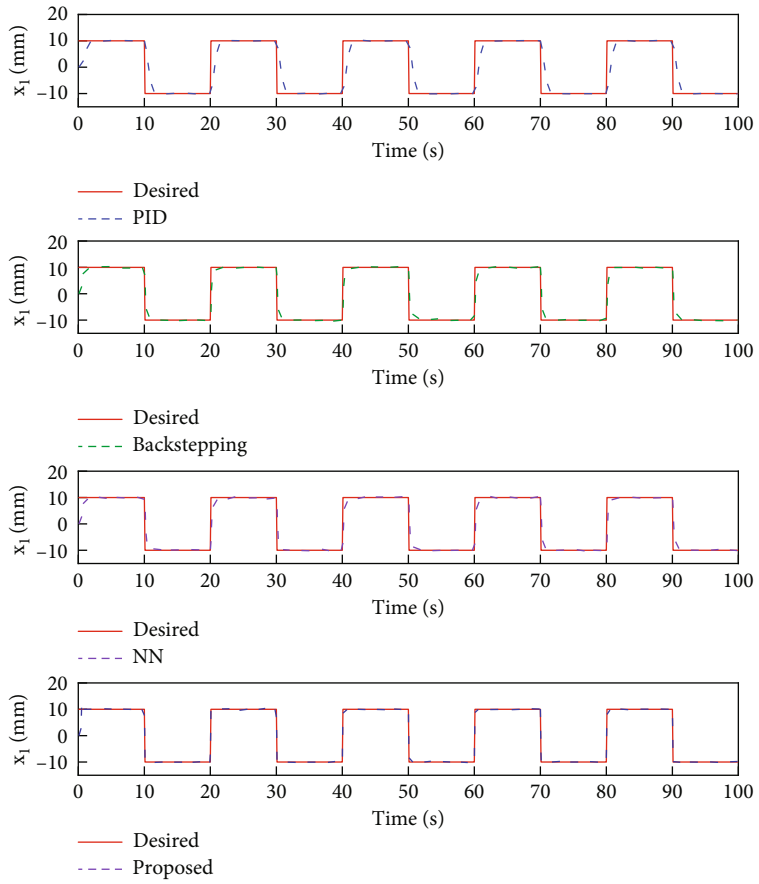

Figure 11: Tracking performance of square signal.

To remove the effect of the known error $x_3^c - x_3^d$, the compensation signal is designed as

$$\dot{z}_2 = -k_2 z_2 - g_1 z_1 + g_2 z_3 + g_2\left(x_3^c - x_3^d\right), \quad z_2(0) = 0, \tag{26}$$

where z_3 will be defined in the next step.

The compensation error signal is described as

$$v_2 = e_2 - z_2. \tag{27}$$

The prediction error is defined as

$$\bar{z}_2 = x_2 - \hat{x}_2. \tag{28}$$

Then, the NN estimation model is constructed as

$$\hat{x}_2 = \hat{\boldsymbol{W}}_2^T \boldsymbol{\Phi}_2(\boldsymbol{X}_2) + g_2 x_3 + \beta_2 \bar{z}_2, \quad \hat{x}_2(0) = x_2(0), \tag{29}$$

where β_2 is the positive design constant.

The adaptive law of RBF NN is designed as

$$\dot{\hat{\boldsymbol{W}}}_2 = \gamma_2\left[(v_2 + \gamma_{z2}\bar{z}_2)\boldsymbol{\Phi}_2(\boldsymbol{X}_2) - \delta_2 \hat{\boldsymbol{W}}_2\right], \tag{30}$$

where γ_2, γ_{z2}, and δ_2 are the positive design constants.

Step 3: Considering the second equation in (6) and using RBF NN to approximate $f_3(x_3)$, it yields

$$\begin{aligned}\dot{x}_3 &= g_3(x_1, x_2, x_3)u + f_1(x_1, x_2, x_3) \\ &= g_1(x_1, x_2, x_3)u + \boldsymbol{W}_3^{*T}\boldsymbol{\Phi}_3(\boldsymbol{X}_3) + \varepsilon_3,\end{aligned} \tag{31}$$

where $\boldsymbol{W}_3^*$ and ε_3 are optimal weight vector and approximation error, respectively.

Define the tracking error

$$e_3 = x_3 - x_3^c. \tag{32}$$

The virtual control is chosen as

$$x_3^d = \frac{\hat{\boldsymbol{W}}_2^T \boldsymbol{\Phi}_2(\boldsymbol{X}_2) - k_2 e_2 + \dot{x}_2^c}{g_2}, \tag{33}$$

where $\hat{\boldsymbol{W}}_2$ is the estimation of $\boldsymbol{W}_2^*$ and k_2 is the positive design constant.

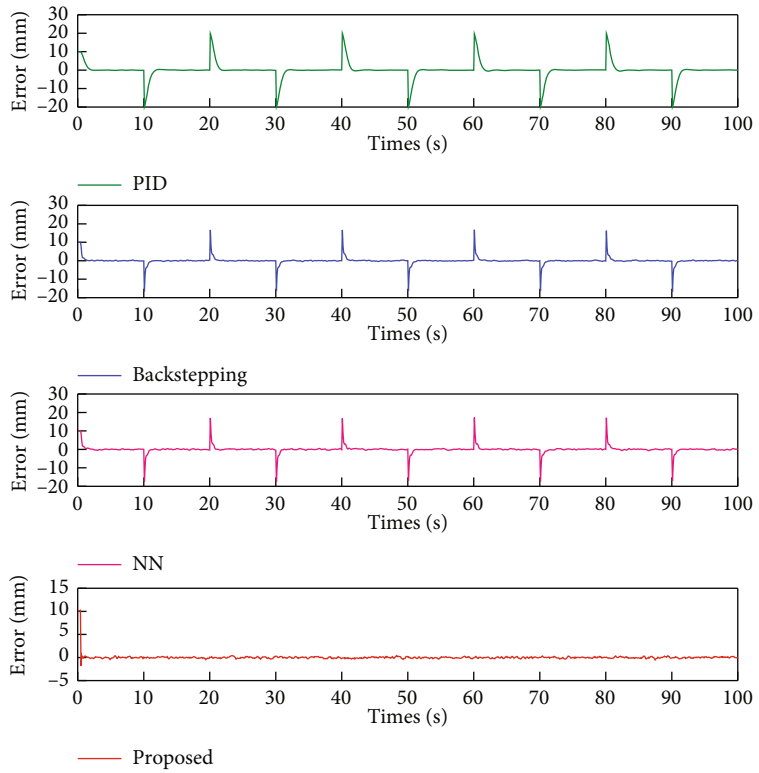

Figure 12: Tracking error of square signal.

Introduce a new state variable x_3^c, and let x_3^d pass through a first-order filter

$$\begin{aligned} \alpha_3 \dot{x}_3^c + x_3^c &= x_3^d, \\ x_3^c(0) &= x_3^d(0), \end{aligned} \tag{34}$$

where α_3 is the positive time constant.

Define $e_3 = x_3 - x_3^c$, and then, the time derivative of e_3 is obtained as

$$\dot{e}_3 = \dot{x}_3 - \dot{x}_3^c = \hat{\boldsymbol{W}}_3^T \boldsymbol{\Phi}_3(\boldsymbol{X}_3) + \varepsilon_3 + x_3 - \dot{x}_3^c = \tilde{\boldsymbol{W}}_3^T \boldsymbol{\Phi}_3(\boldsymbol{X}_3) + \varepsilon_3 - k_3 e_3 - e_2, \tag{35}$$

where $\tilde{\boldsymbol{W}}_3 = \boldsymbol{W}_3^* - \hat{\boldsymbol{W}}_3$.

The compensation signal is designed as

$$\begin{aligned} \dot{z}_3 &= -k_3 z_3 - g_2 z_2, \\ z_3(0) &= 0. \end{aligned} \tag{36}$$

The compensation error signal is described as

$$v_3 = e_3 - z_3. \tag{37}$$

The prediction error is defined as

$$\bar{z}_3 = x_3 - \hat{x}_3. \tag{38}$$

Then, the NN estimation model is constructed as

$$\begin{aligned} \hat{x}_3 &= \hat{\boldsymbol{W}}_3^T \boldsymbol{\Phi}_3(\boldsymbol{X}_3) + g_3 u + \beta_3 \bar{z}_3, \\ \hat{x}_3(0) &= x_3(0), \end{aligned} \tag{39}$$

where β_3 is the positive design constant.

The adaptive law of RBF NN is designed as

$$\dot{\hat{\boldsymbol{W}}}_3 = \gamma_3 \left[(v_3 + \gamma_{z3} \bar{z}_3) \boldsymbol{\Phi}_3(\boldsymbol{X}_3) - \delta_3 \hat{\boldsymbol{W}}_3 \right], \tag{40}$$

where γ_3, γ_{z3}, and δ_3 are the positive design constants.

In the above design process, the RBF NN is employed to approximate state variable, and the prediction error is used for parameter adjustment. The δ modification is adopted to improve the robustness. Compared with traditional backstepping method, the command filter adopted in the proposed control scheme produces certain command signals and their derivatives. In addition, the predication and compensated tracking error is introduced in NN adaptive law to enhance the adaptive capability. Hence, the block diagram of the control system is summarized in Figure 3.

3.3. Stability Analysis. Define the Lyapunov function is as follows

$$\begin{aligned} V = \frac{1}{2}\left(v_1^2 + v_2^2 + v_3^2\right) + \frac{1}{2}\left(\tilde{\boldsymbol{W}}_1^T \gamma_1^{-1} \tilde{\boldsymbol{W}}_1 + \tilde{\boldsymbol{W}}_2^T \gamma_2^{-1} \tilde{\boldsymbol{W}}_2 + \tilde{\boldsymbol{W}}_3^T \gamma_3^{-1} \tilde{\boldsymbol{W}}_3\right) \\ + \frac{1}{2}\left(\gamma_{z1} \bar{z}_1^2 + \gamma_{z2} \bar{z}_2^2 + \gamma_{z3} \bar{z}_3^2\right). \end{aligned} \tag{41}$$

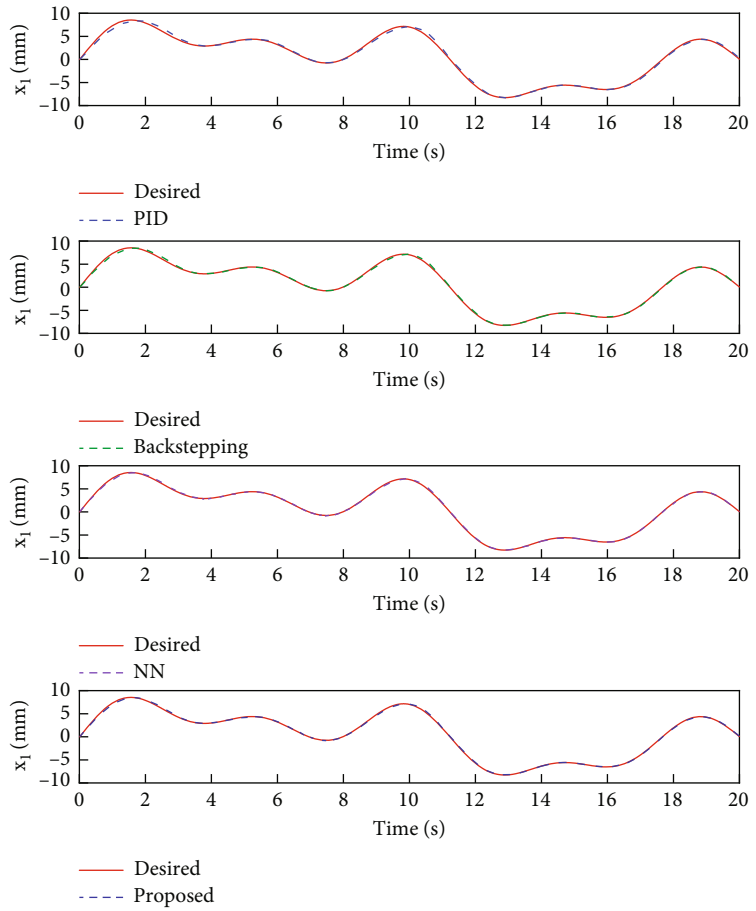

Figure 13: Tracking performance of multifrequency sine signal.

The derivative of V is derived as

$$\dot{V} = (v_1\dot{v}_1 + v_2\dot{v}_2 + v_3\dot{v}_3) - \left(\tilde{W}_1^T\gamma_1^{-1}\dot{\hat{W}}_1 + \tilde{W}_2^T\gamma_2^{-1}\dot{\hat{W}}_2 + \tilde{W}_3^T\gamma_3^{-1}\dot{\hat{W}}_3\right) + \left(\gamma_{z1}\bar{z}_1\dot{\bar{z}}_1 + \gamma_{z2}\bar{z}_2\dot{\bar{z}}_2 + \gamma_{z3}\bar{z}_3\dot{\bar{z}}_3\right). \tag{42}$$

Based on the following facts

$$\dot{v}_i = \dot{e}_i - \dot{z}_i = W_i^T\Phi_i(X_i) - k_iv_i - v_{i-1} + v_{i+1}, \qquad \dot{z}_i = W_i^T\Phi_i(X_i) - \varepsilon_i - \beta_i\bar{z}_i. \tag{43}$$

Then, Equation (42) can be represented as

$$\begin{aligned}\dot{V} = &-\left(k_1v_1^2 + k_2v_2^2 + k_3v_3^2\right) + \left(v_1\varepsilon_1 + v_2\varepsilon_2 + v_3\varepsilon_3\right)\\ &+ \left(\gamma_{z1}\bar{z}_1\varepsilon_1 + \gamma_{z2}\bar{z}_2\varepsilon_2 + \gamma_{z3}\bar{z}_3\varepsilon_3\right)\\ &- \left(\delta_1\beta_1\bar{z}_1^2 + \delta_2\beta_2\bar{z}_2^2 + \delta_3\beta_3\bar{z}_3^2\right)\\ &- \left(\delta_1\tilde{W}_1^T\tilde{W}_1 + \delta_2\tilde{W}_2^T\tilde{W}_2 + \delta_3\tilde{W}_3^T\tilde{W}_3\right)\\ &+ \left(\delta_1\tilde{W}_1^T\tilde{W}_1^* + \delta_2\tilde{W}_2^T\tilde{W}_2^* + \delta_3\tilde{W}_3^T\tilde{W}_3^*\right).\end{aligned} \tag{44}$$

Considering the following facts

$$\begin{aligned}v_i\varepsilon_i - k_iv_i^2 &= k_i\left(v_i - \frac{\varepsilon_i}{2k_i}\right)^2 + \frac{1}{4k_i}\varepsilon_i^2,\\ \bar{z}_i\varepsilon_i - \beta_i\bar{z}_i^2 &= -\beta_i\left(\bar{z}_i - \frac{\varepsilon_i}{2\beta_i}\right)^2 + \frac{1}{4\beta_i}\varepsilon_i^2,\\ \tilde{W}_i^T\tilde{W}_i^* - \tilde{W}_i^T\tilde{W}_i &= -\left\|\tilde{W}_i - \frac{\tilde{W}_i^*}{2}\right\| + \frac{1}{4}\left\|\tilde{W}_i^*\right\|.\end{aligned} \tag{45}$$

Then, Equation (44) can be rewritten as

$$\begin{aligned}\delta_i\left[\left\|\tilde{W}_i - \frac{W_i^*}{2}\right\|^2 - \frac{1}{4}\|W_i^*\|^2\right] \le &-\sum_{i=1}^{3}\left[k_{\min}\left(v_i - \frac{\varepsilon_i}{2k_i}\right)^2\right.\\ &\left.+ \gamma_{z\,\min}\beta_{\min}\left(\bar{z}_i - \frac{\varepsilon_i}{2\beta_i}\right)^2 + \delta_{\min}\left\|\tilde{W}_i - \frac{W_i^*}{2}\right\|^2\right] + \frac{3}{4k_{\min}}\varepsilon_M^2\\ &+ \frac{3\gamma_{z\,\max}}{4\beta_{\min}}\varepsilon_M^2 + \frac{3\delta_{\max}}{4}W_{\max}^2,\end{aligned} \tag{46}$$

where $k_{\min} = \min[k_i]$, $\beta_{\min} = \min[\beta_i]$, $\delta_{\min} = \min[\delta_i]$, $\gamma_{z\,\min}$

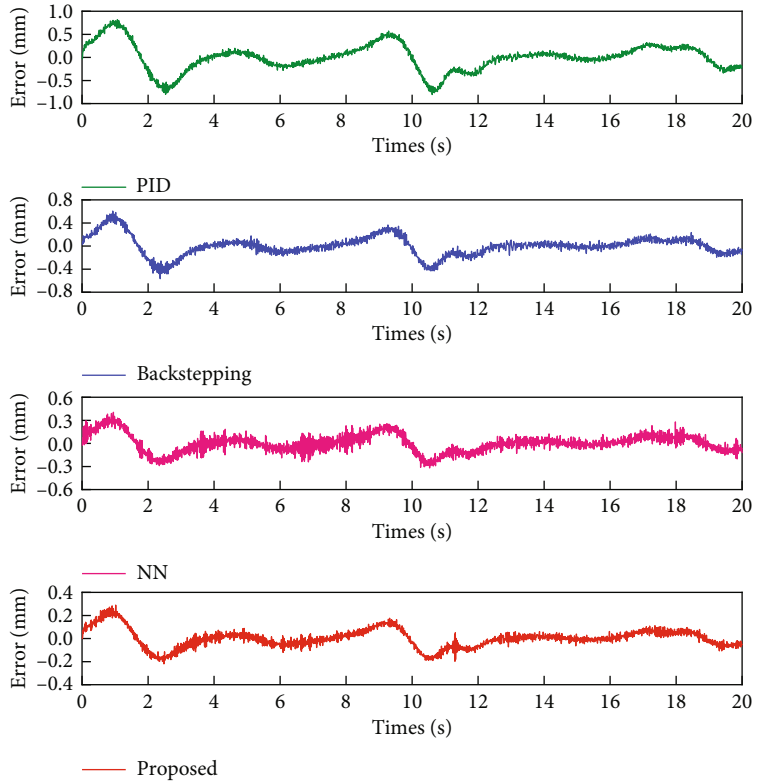

Figure 14: Tracking error of multifrequency sine signal.

$= \min[\gamma_{zi}]$, $\delta_{\max} = \max[\delta_i]$, $\gamma_{z\max} = \max[\gamma_{zi}]$, and $W_{\max} = \max \|\boldsymbol{W}_i^*\|$.

For convenience, define $U = 3\varepsilon_M^2/(4k_{\min}) + 3\gamma_{z\max}\varepsilon_M^2/(4\beta_{\min}) + 3\delta_{\max}\boldsymbol{W}_{\max}^2/4$. If $|v_i - \varepsilon_i/(2k_i)| \geq \sqrt{U/k_0}$, $|\bar{z}_i - \varepsilon_i/(2\beta_i)| \geq \sqrt{U/(\gamma_{z\min}\beta_{\min})}$, and $\|\tilde{\boldsymbol{W}}_i - \boldsymbol{W}_i^*/2\| \geq \sqrt{U/\delta_{\min}}$, it can be found that $\dot{V} \leq 0$. By increasing the values of k_i and β_i, the v_i and $\bar{z}_i$ are all uniformly ultimately bounded and will converge to a small compact set.

4. Simulation Results

To verify the effectiveness of the proposed control scheme, simulations are first performed in MATLAB/Simulink, where *S* function and blocks are used to construct dynamic model and controller. The parameters of hydraulic system are selected as $m = 500\,\text{kg}$, $V_t = 9 \times 10^{-5}\,\text{m}^3$, $\rho = 900\,\text{kg/m}^3$, $A = 3 \times 10^{-4}\,\text{m}^2$, $K = 1500\,\text{N/m}$, $B = 1200\,\text{N}\cdot\text{s/m}$, $C_t = 4 \times 10^{-3}$, $K_{sv} = 6 \times 10^{-7}\,\text{m/V}$, $C_d = 0.62$, and $\beta_e = 7 \times 10^8\,\text{Pa}$. In addition, PID controller, backstepping controller, and NN controller are also test for comparison.

(1) PID: The PID controller is widely used in industrial. The control input is described as

$$u = k_p e_1(t) + k_i \int e_1(t)\mathrm{d}t + k_d \frac{\mathrm{d}e_1(t)}{\mathrm{d}t}, \tag{47}$$

where proportional gain $k_p = 2000$, integral gain $k_i = 500$, and differential gain $k_d = 0.5$. The PID gains are determined via intelligent optimization algorithm to obtain excellent tracking performance.

(2) Backstepping: The backstepping control law is given as

$$u = -\frac{1}{g_3}\left(k_3\bar{z}_3 + f_3 + g_2\bar{z}_2 + \frac{S_2}{\tau_2}\right), \tag{48}$$

where S_2 and τ_2 are dynamic surface and dynamic surface time constant for the second subsystem.

(3) NN: Based on backstepping, the NN control law is designed as

$$u = -k_3\bar{z}_3 - \bar{z}_2 + W_3^T\boldsymbol{\Phi}_3(\boldsymbol{X}_3). \tag{49}$$

(4) Proposed: The main parameters of proposed controller are chosen as $k_i = 40$, $\gamma_i = 20$, $\delta_i = 0.001$, $\alpha_i = 0.002$, $\beta_i = 2$, and $\gamma_{zi} = 0.5$

The tracking performance and tracking error of multifrequency sine signal $y = 5\sin(5\,t) + 2\sin(12.5\,t)$ are shown

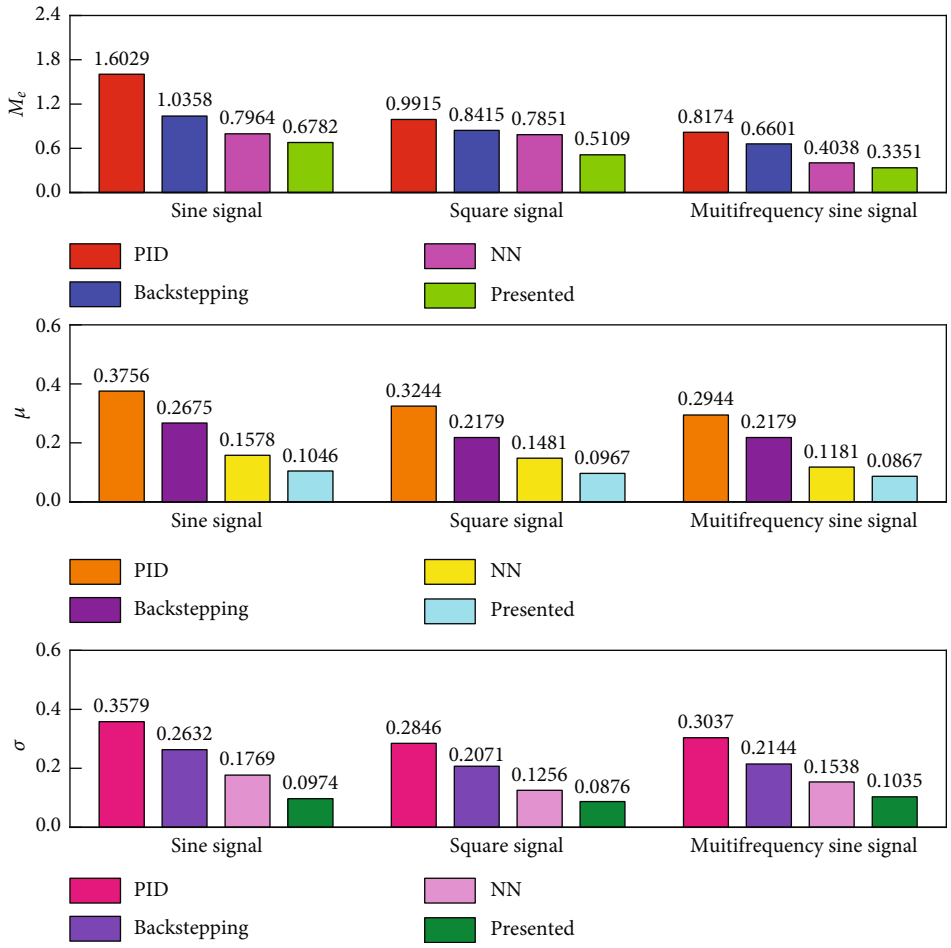

Figure 15: Performance indices of different controllers for the above three cases.

in Figures 4 and 5. The results show that the proposed controller has better dynamic performance than the other three controllers; the tracking error of PID controller is relatively large, i.e., about 0.6 mm; and the tracking error under the backstepping controller and NN controllers is 0.37 mm and 0.3 mm, which are better than the PID controller. The tracking error of the proposed controller is only about 0.2 mm. To investigate the tracking accuracy, three quantitative performance indices are introduced to compare the effects of different controllers, i.e., the maximum tracking error M_e, average tracking error μ, and standard deviation of the tracking error σ. The compared results are listed in Table 1. Clearly, the developed controller generates smaller M_e, μ, and σ than the other three controllers. The NN produces better control performance than backstepping and PID. Thus, the comparative results demonstrate the advantages of the proposed controller.

The position tracking performance of the four controllers for square signal motion is shown in Figure 6. The corresponding performance indicators are demonstrated in Table 2. It can be found that the tracking performance of proposed controller is apparently superior to the other controllers. As it can be seen, the presented controller produces relatively satisfied tracking performance, while PID has a larger tracking error than others. It can be found that the tracking error of the backstepping and NN is smaller than the PID controller. This is reasonable since the NN can handle the nonlinearities and disturbance of EHSS. It should be noted that the M_e for square input signal is replaced by normalized M_e, which is done just for eliminating the effects of amplitude mutations.

5. Experiment Results

To further illustrate the priority of the proposed controller, an experimental platform has been set up as shown in Figure 7. The host computer sends the command signal to the control system by Ethernet using TCP/IP protocol. The proposed control scheme is programed by MATLAB/Simulink software. The controller drives the hydraulic servo system to produce the desired motion by controlling the opening of servo valve. The position and pressure signals of EHSS obtained by sensor are sent to the signal modulator to constitute the feedback loop. The sample rate of the controller for the EHSS is set to 1000 Hz.

Figures 8 and 9 show comparison results among PID controller, backstepping controller, NN controller, and proposed controller for the tracking performance of the sine

signal $y = 5\sin(2\pi t)$. It can be found that the maximum steady-state tracking error of the proposed controller is less 0.18 mm, which is small than that of backstepping controller (0.5 mm) and NN controller (0.4 mm). As a comparison, the maximum steady-state tracking error of PID controller is 0.8 mm. It is indicated that the proposed controller achieves best control performance for sine signal. Moreover, Figure 10 provides the control signal of four controllers. It can be found that the control signal of presented is more smooth than that the other three controller, which helps to reduce chattering and phase lag. From these comparative results, one can confirm that the developed controller can effectively handle the nonlinearities and disturbances.

The tracking performance and tracking error of square signal for different controllers are shown in Figures 11 and 12. From these results, one can find that the tracking error of the presented method is smaller than PID, backstepping, and NN schemes, since fast convergence of the estimated parameters can be retained by using adaptive control law. Thus, the proposed method has better ability than the other three controllers in dealing with modeling uncertainties and external disturbances even under abrupt load variation.

The tracking performance and the tracking error curve of multifrequency sine signal $y = 5\sin(0.1\pi t) + 4\sin(0.25\pi t) + 3\sin(0.45\pi t)$ are presented in Figures 13 and 14. Obviously, the proposed controller exhibits best tracking performance than the other controllers, where the tracking error is less than 0.3 mm. The tracking error of the PID controller is kept in 0.8 mm. In contrast, the backstepping controller and NN controller has smaller error, within 0.6 mm and 0.4 mm, respectively.

The performance indices of different controllers for the above three cases are shown in Figure 15. One can find that the values of M_e for sine input signal for four controllers are 1.6029 mm, 1.0358 mm, 0.7964 mm, and 0.6782 mm, respectively, which indicates that the maximum tracking error of the proposed controller is decreased by 57.68%. Similar results are capable to be found in square signal and multifrequency sine signal in all cases.

6. Conclusion

In this paper, an adaptive backstepping control method based on NN is proposed for the EHSS position tracking under modeling uncertainties and external disturbances. Based on the dynamic model of EHSS, the proposed controller is designed by the adaptive backstepping and neural network approximation. The backstepping control is utilized to handle modeling uncertainties and external disturbances. The NN is used to approximate the unknown and continuous function in the design process. The uniform stability is proved by Lyapunov method. Extensive simulation and experimental results show that the proposed control strategy can improve the tracking accuracy in the presence of modeling uncertainties and external disturbance. In addition, dynamic state constraints and output constraints problem due to physical limitation and performance requirement of hydraulic system will be further study.

Data Availability

The data used to support the findings of this study are included within the article.

Conflicts of Interest

The authors declare that they have no conflicts of interest.

Acknowledgments

This research was funded by the Key Science and Technology Program of Henan Province (222102220104) and the High-Level Talent Foundation of Henan University of Technology (2020BS043).

References

[1] X. W. Yang, J. Y. Yao, and W. X. Deng, "Output feedback adaptive super-twisting sliding mode control of hydraulic systems with disturbance compensation," *ISA Transactions*, vol. 109, pp. 175–185, 2021.

[2] J. Y. Yao, "Model-based nonlinear control of hydraulic servo systems: challenges, developments and perspectives," *Frontiers of Mechanical Engineering*, vol. 13, no. 2, pp. 179–210, 2018.

[3] W. X. Deng, J. Y. Yao, Y. Y. Wang, X. W. Yang, and J. H. Chen, "Output feedback backstepping control of hydraulic actuators with valve dynamics compensation," *Mechanical Systems and Signal Processing*, vol. 158, pp. 1–18, 2021.

[4] M. E. M. Essa, M. A. S. Aboelela, M. A. M. Hassan, and S. M. Abdrabbo, "Model predictive force control of hardware implementation for electro-hydraulic servo system," *Transactions of the Institute of Measurement and Control*, vol. 41, no. 5, pp. 1435–1446, 2019.

[5] H. B. Yuan, H. C. Na, and Y. B. Kim, "System identification and robust position control for electro-hydraulic servo system using hybrid model predictive control," *Journal of Vibration and Control*, vol. 24, no. 18, pp. 4145–4159, 2018.

[6] J. Yang, J. Na, Y. Guo, and X. Wu, "Adaptive estimation of road gradient and vehicle parameters for vehicular systems," *IET Control Theory and Applications*, vol. 9, no. 6, pp. 935–943, 2015.

[7] Z. L. Chen, Q. Guo, H. Y. Xiong, D. Jiang, and Y. Yan, "Control and implementation of 2-DOF lower limb exoskeleton experiment platform," *Chinese Journal of Mechanical Engineering*, vol. 34, no. 1, pp. 1–17, 2021.

[8] L. K. Zhu, Z. B. Wang, H. Qiang, and Y. Q. Liu, "Global sliding-mode dynamic surface control for MDF continuous hot-pressing slab thickness via LESO," *International Journal of Machine Learning and Cybernetics*, vol. 10, no. 6, pp. 1249–1258, 2019.

[9] Y. Chu, Z. Yuan, X. He, and Z. Dong, "Model construction and performance degradation characteristics of a deflector jet pressure servo valve under the condition of oil contamination," *International Journal of Aerospace Engineering*, vol. 2021, Article ID 8840084, 17 pages, 2021.

[10] B. Xu, J. Shen, S. Liu, Q. Su, and J. Zhang, "Research and development of electro-hydraulic control valves oriented to industry 4.0: a *review*," *Mechanical Engineering*, vol. 33, no. 1, pp. 1–20, 2020.

[11] M. Zhang, R. Jiang, and H. Nie, "Design and test of dual actuator nose wheel steering system for large civil aircraft,"

International Journal of Aerospace Engineering, vol. 2016, Article ID 1626015, 14 pages, 2016.

[12] G. Shen, Z. C. Zhu, X. Li, Q. G. Wang, G. Li, and Y. Tang, "Acceleration waveform replication on six-degree-of-freedom redundant electro-hydraulic shaking tables using an inverse model controller with a modelling error," *Transactions of the Institute of Measurement and Control*, vol. 40, no. 3, pp. 968–986, 2018.

[13] H. Pan, W. Sun, X. Jing, H. Gao, and J. Yao, "Adaptive tracking control for active suspension systems with non-ideal actuators," *Journal of Sound and Vibration*, vol. 399, pp. 2–20, 2017.

[14] W. X. Deng and J. Y. Yao, "Asymptotic tracking control of mechanical servosystems with mismatched uncertainties," *IEEE-ASME Transactions on Mechatronics*, vol. 26, no. 4, pp. 2204–2214, 2021.

[15] J. Y. Yao, W. X. Deng, and W. C. Sun, "Precision motion control for electro-hydraulic servo systems with noise alleviation: a desired compensation adaptive approach," *IEEE-ASME Transactions on Mechatronics*, vol. 22, no. 4, pp. 1859–1868, 2017.

[16] Q. Guo, T. Yu, and D. Jiang, "High-gain observer-based output feedback control of single-rod electro- hydraulic actuator," *IET Control Theory and Applications*, vol. 9, no. 16, pp. 2395–2404, 2015.

[17] Q. Guo, Y. L. Liu, D. Jiang et al., "Prescribed performance constraint regulation of electrohydraulic control based on backstepping with dynamic surface," *Applied Sciences-Basel*, vol. 8, no. 1, pp. 16–76, 2018.

[18] C. Yang, F. Yao, M. J. Zhang, Z. Q. Zhang, Z. Z. Wu, and P. J. Dan, "Adaptive sliding mode PID control for underwater manipulator based on Legendre polynomial function approximation and its experimental evaluation," *Applied Sciences-Basel*, vol. 10, no. 5, pp. 1715–1728, 2020.

[19] C. Kaddissi, J. P. Kenne, and M. Saad, "Identification and real-time control of an electrohydraulic servo system based on nonlinear backstepping," *IEEE-ASME Transactions on Mechatronics*, vol. 12, no. 1, pp. 12–22, 2007.

[20] X. D. Li, X. Chen, and C. S. Zhou, "Combined observer-controller synthesis for electro-hydraulic servo system with modeling uncertainties and partial state feedback," *Journal of the Franklin Institute-Engineering and Applied Mathematics*, vol. 355, no. 13, pp. 5893–5911, 2018.

[21] Z. B. Xu, D. W. Ma, J. Y. Yao, and N. Ullah, "Feedback nonlinear robust control for hydraulic system with disturbance compensation," *Proceedings of the Institution of Mechanical Engineers Part I-Journal of Systems and Control Engineering*, vol. 230, no. 9, pp. 978–987, 2016.

[22] X. X. Yin, W. C. Zhang, Z. S. Jiang, and L. Pan, "Adaptive robust integral sliding mode pitch angle control of an electro-hydraulic servo pitch system for wind turbine," *Mechanical Systems and Signal Processing*, vol. 133, pp. 1–15, 2019.

[23] J. Na, X. M. Ren, G. Herrmann, and Z. Qiao, "Adaptive neural dynamic surface control for servo systems with unknown dead- zone," *Control Engineering Practice*, vol. 19, no. 11, pp. 1328–1343, 2011.

[24] S. B. Wang, J. Na, and Y. S. Xing, "Adaptive optimal parameter estimation and control of servo mechanisms: theory and experiments," *IEEE Transactions on Industrial Electronics*, vol. 68, no. 1, pp. 598–608, 2021.

[25] L. Yu, S. Fei, J. Huang, and Z. Hou, "Sliding mode switching control under arbitrary switchings in the presence of uncertain parameters," *Proceedings of the Institution of Mechanical Engineers Part I-Journal of Systems and Control Engineering*, vol. 232, no. 4, pp. 399–407, 2018.

[26] L. Qiao and W. D. Zhang, "Trajectory tracking control of AUVs via adaptive fast nonsingular integral terminal sliding mode control," *IEEE Transactions on Industrial Informatics*, vol. 16, no. 2, pp. 1248–1258, 2020.

[27] M. X. Yang, Q. Zhang, X. L. Lu, R. R. Xi, and X. S. Wang, "Adaptive sliding mode control of a nonlinear electro-hydraulic servo system for position tracking," *Mechanika*, vol. 25, no. 4, pp. 283–290, 2019.

[28] Q. Guo, Y. Zhang, B. G. Celler, and S. W. Su, "Backstepping control of electro-hydraulic system based on extended-state-observer with plant dynamics largely unknown," *IEEE Transactions on Industrial Electronics*, vol. 63, no. 11, pp. 6909–6920, 2016.

[29] Z. Chen, F. H. Huang, C. N. Yang, and B. Yao, "Adaptive fuzzy backstepping control for stable nonlinear bilateral teleoperation manipulators with enhanced transparency performance," *IEEE Transactions on Industrial Electronics*, vol. 67, no. 1, pp. 746–756, 2020.

[30] X. W. Yang, W. X. Deng, and J. Y. Yao, "Neural network based output feedback control for DC motors with asymptotic stability," *Mechanical Systems and Signal Processing*, vol. 164, pp. 1–15, 2022.

[31] Z. Chen, F. Huang, W. Sun, J. Gu, and B. Yao, "RBF-neural-network-based adaptive robust control for nonlinear bilateral teleoperation manipulators with uncertainty and time delay," *IEEE-ASME Transactions on Mechatronics*, vol. 25, no. 2, pp. 906–918, 2020.

[32] J.-H. Park, S.-H. Kim, and T.-S. Park, "Output-feedback adaptive neural controller for uncertain pure-feedback nonlinear systems using a high-order sliding mode observer," *IEEE Transactions on Neural Networks and Learning Systems*, vol. 30, no. 5, pp. 1596–1601, 2019.

[33] S. Wang, "Approximation-free control for nonlinear helicopters with unknown dynamics," *IEEE Transactions on Circuits and Systems Ii-Express Briefs*, vol. 69, no. 7, pp. 3254–3258, 2022.

[34] S. Chen, Z. Chen, B. Yao et al., "Adaptive robust cascade force control of 1-DOF hydraulic exoskeleton for human performance augmentation," *IEEE-ASME Transactions on Mechatronics*, vol. 22, no. 2, pp. 589–600, 2017.

[35] C. Cheng, S. Y. Liu, and H. Z. Wu, "Sliding mode observer-based fractional-order proportional-integral-derivative sliding mode control for electro-hydraulic servo systems," *Proceedings of the Institution of Mechanical Engineers Part C-Journal of Mechanical Engineering Science*, vol. 234, no. 10, pp. 1887–1898, 2020.

[36] W. Liu, C.-C. Lim, P. Shi, and S. Xu, "Backstepping fuzzy adaptive control for a class of quantized nonlinear systems," *IEEE Transactions on Fuzzy Systems*, vol. 25, no. 5, pp. 1090–1101, 2017.

[37] J. Na, X. M. Ren, C. Shang, and Y. Guo, "Adaptive neural network predictive control for nonlinear pure feedback systems with input delay," *Journal of Process Control*, vol. 22, no. 1, pp. 194–206, 2012.

[38] X. Yang, W. Deng, and J. Yao, "Neural adaptive dynamic surface asymptotic tracking control of hydraulic manipulators with guaranteed transient performance," *IEEE Transactions*

on Neural Networks and Learning Systems, vol. PP, pp. 1–11, 2022.

[39] G. Li, J. Na, D. P. Stoten, and X. M. Ren, "Adaptive neural network feedforward control for dynamically substructured systems," *IEEE Transactions on Control Systems Technology*, vol. 22, no. 3, pp. 944–954, 2014.

[40] F. J. Luan, J. Na, Y. B. Huang, and G. B. Gao, "Adaptive neural network control for robotic manipulators with guaranteed finite-time convergence," *Neurocomputing*, vol. 337, pp. 153–164, 2019.

[41] L. Liu, Y.-J. Liu, and S. Tong, "Neural networks-based adaptive finite-time fault-tolerant control for a class of strict-feedback switched nonlinear systems," *IEEE Transactions on Cybernetics*, vol. 49, no. 7, pp. 2536–2545, 2019.